TWO DIMENSIONAL ANALYSIS OF THE CRYSTALLIZATION OF HOLLOW COMPOUND PLASTIC FIBERS

Francisco J. Blanco-Rodríguez[a], J.I. Ramos[a,*]

[a] Escuela de Ingenierías, Doctor Ortíz Ramos, s/n, Universidad de Málaga, 29071, Málaga, Spain
*Corresponding author: Fax: +34 951 952 542 Email: jirs@lcc.uma.es

ABSTRACT

A quasi-two-dimensional model of the melt spinning of hollow, compound plastic fibers is presented. The model is based on the leading-order one-dimensional equations for the fiber's geometry and axial and radial velocity components obtained by means of a perturbation method for slender Newtonian fibers at low Reynolds numbers, and two-dimensional equations for the temperature, molecular orientation and crystallization. Due to the nonlinear dependence of the viscosity on the temperature, the model is governed by a set of integro-differential equations. It is shown that a thermal boundary layer is formed at the outer surface of the outer fiber and that the fiber reaches constant diameters on account of the increase of dynamic viscosity as the temperature decreases. It is also shown that, for the conditions analyzed here, the flow-induced crystallization is much smaller than the thermal one.

INTRODUCTION

Membrane separation processes are employed in a variety of industries ranging from water treatment to industrial gas separation. These processes usually employ polymeric membranes in either hollow fiber or flat sheet forms. The hollow fiber is broadly used because of its high surface-to-volume ratio and is the preferred form in ultrafiltration, dialysis, and gas separation processes. Hollow fibers are also used in the textile industry as well as in optics, e.g., micro-structured optical fibers, for infrared imaging and sensing, wave transmission, etc., in military and medical applications, etc. [1, 2, 3].

Hollow compound fibers are hollow fibers that consist of inner and outer materials; the outer material may have different mechanical, chemical, optical, etc., characteristics than the inner one, or may serve simply as a protection. The combination of two or more different materials with different properties may result in composite fibers with highly desireable properties.

Although some one-dimensional models have been developed to study the melt spinning of single-component hollow fibers [3, 4, 5, 6, 7] based on Taylor's series expansions in the radial direction, asymptotic methods or integral formulations of the governing equations for slender fibers under isothermal and non-isothermal conditions, there have been few studies on the melt spinning of hollow, compound fibers [3, 8, 9] and these studies have been limited to the very small Biot numbers for which an asymptotic analysis for slender fibers indicates that the temperature across the fiber is uniform at leading-order. For moderate or large Biot numbers, such a uniform temperature approximation is not expected to be valid, especially at the interfaces between the fiber and its surrounding media and at the interface between the inner and outer fibers that make the hollow, compound fiber. These temperature uniformities, in turn, affect the velocity field through the dependence of the dynamic viscosity on the temperature, and the molecular orientation and crystallization of semicrystalline polymer fibers through their dependence on the thermal field and the strain and stress tensors. As a consequence, temperature non-uniformities across a hollow, compound fiber may result in non-uniformities on the degrees of molecular orientation and crystallization which, in turn, affect the fiber's morphology and properties.

In this paper, we present a quasi-two-dimensional model of the melt spinning of hollow, compound semi-crystalline polymeric fibers based on the leading-order equations for the fiber's geometry and axial and radial velocity components obtained from an asymptotic analysis for slender fibers at low

Reynolds numbers and two-dimensional equations for the temperature, molecular orientation and crystallization. The model employs a Newtonian rheology, an order parameter deduced from the Doi-Edwards equation for the tensor of orientation, and the thermal Avrami-Kolmogorov crystallization kinetics modified by the effects of the flow-induced crystallization.

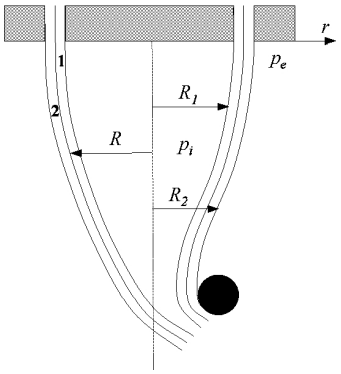

Figure 1
Schematic of hollow compound liquid jet/fiber.

FORMULATION

Consider an axisymmetric, hollow, compound liquid jet such as the one shown schematically in Figure 1, consisting of two immiscible, incompressible (constant density) Newtonian fluids. The inner and outer jets correspond to $R_1(t,x) \le r \le R(t,x)$ and $R(t,x) \le r \le R_2(t,x)$, respectively, where r, x, and t denote the radial and axial coordinates, and time, respectively. The fluid dynamics of the hollow, compound jet are governed by the conservation equations of mass, linear momentum and energy, and kinematic, dynamic and thermal conditions at the jet's interfaces [8]. In this study, we assume that the density, ρ_i, specific heat, C_i, and thermal conductivity, K_i, are constant, while the dynamic viscosity, μ_i, is a function of the temperature, T_i, through an Arrhenius-type expression and depends on the molecular orientation and degree of crystallization, where $i = 1, 2$ denote the inner and outer hollow fibers, respectively. It is also assumed that the fluids of the inner and outer fiber are Newtonian and that gases surrounding the hollow, compound fiber are dynamically passive, i.e., their pressures, p_i and p_e, are only a function of time, since, in general, they have smaller density and dynamic viscosity than those of liquids. This implies that the gases surrounding the liquid may not introduce strong velocity variations along each cross section of the jet, although they may affect its dynamics. In addition, p_e can be set to zero.

For slender jets at low Reynolds number, i.e., $\varepsilon = R_0 / L << 1$, it is convenient to non-dimensionalize r, x, t, u, v, ρ, C, K and p with respect to R_0, L, L/u_0, u_0, v_0, ρ_0, C_0, K_0 and $\mu_0 u_0 / L$, respectively, where R_0 and L denote a characteristic radius and a characteristic distance in the axial direction, e.g., the die's exit radius and the distance from the die's exit to the take-up point, respectively, u_0 is a characteristic (constant) axial velocity component, $v_0 = \varepsilon u_0$, and ρ_0 and μ_0 are a reference density and viscosity, respectively, and v denotes the radial velocity component. The temperature may be non-dimensionalized as $\hat{T} = (T - T_r)/\Delta T$ where $\Delta T = T_0$ with $T_r = 0$.

Using this non-dimensionalization, it is an easy exercise to show that the non-dimensional equations and boundary conditions depend on ε, and the non-dimensional numbers *Re*, *Fr*, *Ca*, *Pr*, *Br*, *Bi*, where

$$\mathrm{Re} = \frac{\rho_0 u_0 R_0}{\mu_0}, \quad Fr = \frac{u_0^2}{g R_0}, \quad Ca = \frac{\mu_0 u_0}{\sigma}, \tag{1}$$

$$Pe = \mathrm{Re}\,\mathrm{Pr}, \quad \mathrm{Pr} = \frac{\mu_0 C_0}{K_0}, \tag{2}$$

$$Br = \frac{\mu_0 u_0^2}{K_0 \Delta T}, \quad Bi = \frac{h_0 R_0}{K_0}, \tag{3}$$

denote the Reynolds, Froude, capillary, thermal Péclet, Prandtl, Brinkman and Biot numbers, respectively. Note that the surface tensions, σ_i and σ, have been assumed to be constant, and h_0 is a characteristic film heat transfer coefficient.

In addition, the resulting nondimensional conservation equations also depend on the boundary conditions at the die's exit and take-up point. This large set of parameters does not allow us to obtain simpler equations except for slender geometries and small values of the Reynolds, Biot and Brinkman numbers. We, therefore, consider typical operating conditions in the manufacture of hollow, compound fibers which are usually characterized by small values of the Reynolds, Biot and Brinkman numbers.

For small Reynolds numbers, $\mathrm{Re} = \varepsilon \overline{R}$ with $\overline{R} = O(1)$, and $Fr = \overline{F}/\varepsilon$, $Ca = \overline{C}/\varepsilon$, $Bi = \varepsilon^2 \overline{B}$, $Br = \varepsilon^2 \overline{b}$, where $\overline{F} = O(1)$, $\overline{C} = O(1)$, $\overline{B} = O(1)$ and $\overline{b} = O(1)$, which correspond to small gravitational effects, small surface tension, small heat convection and small viscous disipation, expansion of the nondimensional dependent variables $\hat{R}_1$, $\hat{R}$, $\hat{R}_2$, $\hat{u}_i$, $\hat{v}_i$, $\hat{p}_i$ and $\hat{T}_i$, where $i = 1, 2$ as $\phi = \phi_{,0} + \varepsilon^2 \phi_{,2} + O(\varepsilon^4)$, where ϕ denotes dependent variables, into the governing equations and boundary conditions, together with the expansion of the boundary conditions at $\hat{R}_1(t,x)$, $\hat{R}(t,x)$ and $\hat{R}_2(t,x)$ about $\hat{R}_{10}(t,x) \equiv R_1$, $\hat{R}_0(t,x) \equiv R_0$ and $\hat{R}_{20}(t,x) \equiv R_{20}$, respectively, yield asymptotic expansions which, after lengthy algebra and use of the asymptotic equations at $O(\varepsilon^2)$, result in the following leading-order equations for the fiber's geometry

$$\begin{aligned}
&\frac{\partial A_1}{\partial \hat{t}} + \frac{\partial}{\partial \hat{x}}\left(B A_1\right) = 0 \\
&\frac{\partial A_2}{\partial \hat{t}} + \frac{\partial}{\partial \hat{x}}\left(B A_2\right) = 0 \\
&\frac{\partial R_0^2}{\partial \hat{t}} + \frac{\partial}{\partial \hat{x}}\left(B R_0^2\right) = 2C(\hat{x})
\end{aligned} \tag{4}$$

where $2C(\hat{x})$ is given by

$$2C(\hat{x}) = -\frac{1}{\overline{C}} \frac{\left(\frac{\sigma_1}{\sigma}\right)\frac{1}{R_1} + \frac{1}{R_0} + \left(\frac{\sigma_2}{\sigma}\right)\frac{1}{R_2}}{<\hat{\mu}_{e1,0}>\frac{1}{R_1^2} + \left(<\hat{\mu}_{e2,0}> - <\hat{\mu}_{e1,0}>\right)\frac{1}{R_0^2} - <\hat{\mu}_{e2,0}>\frac{1}{R_2^2}} \tag{5}$$

and the following leading-order axial and radial velocity components

$$\begin{aligned}
&\left(\hat{\rho}_1 A_1 + \hat{\rho}_2 A_2\right)\overline{R}\,\frac{DB}{Dt} = \left(\hat{\rho}_1 A_1 + \hat{\rho}_2 A_2\right)\frac{\overline{R}}{\overline{F}} \\
&+ \frac{\partial}{\partial \hat{x}}\left(3\left(<\hat{\mu}_{e1,0}> A_1 + <\hat{\mu}_{e2,0}> A_2\right)\frac{\partial B}{\partial \hat{x}}\right) \\
&+ 2C(\hat{x})\left(-\frac{<\hat{\mu}_{e1,0}>}{R_1}\frac{\partial R_1}{\partial \hat{x}} + \frac{<\hat{\mu}_{e2,0}>}{R_2}\frac{\partial R_2}{\partial \hat{x}}\right) \\
&+ 2C(\hat{x})\left(\frac{<\hat{\mu}_{e1,0}> - <\hat{\mu}_{e2,0}>}{R_0}\frac{\partial R_0}{\partial \hat{x}}\right) \\
&- A_1\frac{\partial D_1}{\partial \hat{x}} - A_2\frac{\partial D_2}{\partial \hat{x}},
\end{aligned} \tag{6}$$

$$\hat{v}_{i,0} = \frac{C(\hat{x})}{\hat{r}} - \frac{\hat{r}}{2}\frac{\partial B}{\partial \hat{x}}, \tag{7}$$

respectively where

$$D_1 = -<\hat{\mu}_{e1,0}>\frac{2C(\hat{x})}{R_1^2} - \frac{1}{\overline{C}}\left(\frac{\sigma_1}{\sigma}\right)\frac{1}{R_1}, \tag{8}$$

$$D_2 = -<\hat{\mu}_{e2,0}>\frac{2C(\hat{x})}{R_2^2} + \frac{1}{\overline{C}}\left(\frac{\sigma_2}{\sigma}\right)\frac{1}{R_2}, \tag{9}$$

B denotes the nondimensional leading-order axial velocity component, and $A_1 = (R_0^2 - R_1^2)/2$ and $A_2 = (R_2^2 - R_0^2)/2$ denote the nondimensional leading-order cross-sectional areas of the inner and outer jets, respectively, and $\frac{DB}{Dt} = \frac{\partial B}{\partial \hat{t}} + B\frac{\partial B}{\partial \hat{x}}$.

The leading-order energy equation is also one-dimensional, i.e., the leading-order temperature is uniform across the hollow, compound fiber. Such an approximation is a consequence of the ordering of the Biot number employed in the asymptotic analysis. For moderate or large Biot numbers, nonuniform temperature distribution at the die's exit, and/or different materials for the inner and outer hollow jets of the compound fiber, such a one-dimensional equation is not valid because the temperature varies in the axial and radial directions. Under these conditions, the use of the slender approximation and the neglect of both the viscous dissipation terms and the work done by the gravitational acceleration allows us to write the following energy equation

$$\begin{aligned}
&\hat{\rho}_i \hat{C}_i \overline{P}\,\mathcal{L}\left(\hat{T}_i\right) \equiv \hat{\rho}_i \hat{C}_i \overline{P}\left(\frac{\partial \hat{T}_i}{\partial \hat{t}} + B\frac{\partial \hat{T}_i}{\partial \hat{x}} + \hat{v}_{i,0}\frac{\partial \hat{T}_i}{\partial \hat{r}}\right) \\
&= \varepsilon^2 \frac{\partial}{\partial \hat{x}}\left(\hat{K}_i \frac{\partial \hat{T}_i}{\partial \hat{x}}\right) + \frac{1}{\hat{r}}\frac{\partial}{\partial \hat{r}}\left(\hat{r}\,\hat{K}_i \frac{\partial \hat{T}_i}{\partial \hat{r}}\right),
\end{aligned} \tag{10}$$

where $\overline{P} = \varepsilon^2 \overline{R}\ \mathrm{Pr} = \varepsilon^2 Pe$, and the axial diffusion term in the energy equation can be neglected for slender fibers.

The inner interface $\hat{r} = R_1$ was assumed adiabatic ($\hat{h}_1 = 0$); at the $\hat{r} = R_0$ interface, the temperature and the heat flux were assumed to be continuous, whereas, at $\hat{r} = R_2$, the heat flux was set equal to the convective one that, for slender fibers, can be written (neglecting terms of $O(\varepsilon^2)$) as

$$-\hat{K}_2 \frac{\partial \hat{T}_2}{\partial \hat{r}}(\hat{t}, R_2, \hat{x}) = \overline{B}\,\hat{h}_2(\hat{T}(\hat{t}, R_2, \hat{x}) - \hat{T}_{2,\infty}),$$

albeit, the boundary conditions were employed at the leading—order geometry.

In the equations presented above, phase changes and the resulting latent heat effects have been neglected, the rheology has been assumed to be Newtonian and molecular orientation and crystallization phenomena have been ignored. The rate of crystallization depends on the molecular orientation in the melt; when subject to deformations that align the polymer molecules, the rate of crystallization increases dramatically, and, when the temperature drops below the glass transition temperature, there is a cessation of molecular motion and the crystallization rate decreases and may stop. As the crystallinity increases, it retards the crystallization process and decreases the mobility of the polymer molecules in the amorphous phase. Moreover, the rate of molecular orientation increases as as the strain rate is increased. This means that the crystallization depends on both thermal and flow-induced effects.

In this paper, we have employed the following generalization of the Avrami-Kolmogorov thermal crystallization theory [11]

$$\mathcal{L}(Y_i) = k_{Ai}(S_i)\,(Y_{\infty,i} - Y_i), \qquad (11)$$

where Y is the degree of crystallinity, $k_{Ai}(S) = k_{Ai}(0)\exp(a_{2i} S_i^2)$ is the linearized growth rate, $k_{Ai}(0)$ is the amorphous growth rate [11], a_{2i} is a constant, $Y_{\infty,i}$ is the ultimate degree of crystallinity, and S is an order parameter that characterizes the degree of orientation defined as the ensemble average of the alignment of the molecular direction to the axial direction and has been determined from the Doi-Edwards equation for the molecular orientation tensor which is, in turn, derived from the probability density function for the molecular orientation by taking moments and approximating the fourth-order moments in terms of second-order ones. By assuming that the traceless orientation tensor is symmetric and setting to zero its $_{r\theta}$ and $_{x\theta}$ components only fourth components are needed to define this tensor. Furthermore, for slender fibers, it is easy to show that the $_{rx}$ component of this tensor is on the order of the slenderness ratio and can, therefore, be neglected for slender fibers; this assumption implies that the molecular orientation tensor can be written as

$$\mathbf{S} = \frac{1}{3}\begin{pmatrix} s_r & 0 & 0 \\ 0 & -(s_r + s_x) & 0 \\ 0 & 0 & s_x \end{pmatrix}, \qquad (12)$$

where

$$\mathcal{L}(s_{ir}) = (1 - s_{ir})(1 + s_{ix})\frac{\partial B}{\partial \hat{x}} - \frac{\psi_i}{\hat{\lambda}_i}\left\{ s_{ir} + \frac{N_i}{3}[(s_{ir} - 1)(s_{ir} - O_i)] \right\}, \qquad (13)$$

$$\mathcal{L}(s_{ix}) = (1 + s_{ix})(2 - s_{ix})\frac{\partial B}{\partial \hat{x}} - \frac{\psi_i}{\hat{\lambda}_i}\left\{ s_{ix} - \frac{N_i}{3}[(s_{ix} + 1)(s_{ix} - O_i)] \right\}, \qquad (14)$$

$$O_i = \frac{2}{3}\left(s_{ir}^2 + s_{ix}^2 - s_{ir} s_{ix}\right), \qquad (15)$$

and $i = 1, 2$, ψ is an anisotropic drag parameter ($0 < \psi \le 1, \psi = 1$ for isotropic models, and $\psi \approx 0.5$ for rigid-rod molecular models), $\hat{\lambda}_i = \hat{\lambda}_{i0}\exp(\omega \cdot (1 - \hat{T}))$ is a linearized form of the Arrhenius model used for the molecular relaxation time of the liquid-crystalline polymer, N_i is the dimensionless density of the liquid-crystalline polymer, β_i is the crystallization viscosity rate and n_i is the crystallization viscosity index which are material-dependent, e.g., $\beta_i = 4.605$ and $n_i = 12$ for nylon-66, $\beta_i = 4$ and $n_i = 2$ for PET.

From Eq. (12), the order parameter becomes

$$S_i^2 = \frac{3}{2}(\mathbf{S} : \mathbf{S}) = \frac{1}{3}\left(s_{ir}^2 + s_{ix}^2 - s_{ir}s_{ix}\right) \qquad (16)$$

which is the expression to be used in the equation for the degree of crystallization.

The initial conditions for the molecular orientation tensor employed in this study are

$$s_{ir}(\hat{r},0) = -\sqrt{\frac{6}{2+\chi^2}}S_{i0}(\hat{r}) \qquad (17)$$

$$s_{ix}(\hat{r},0) = \chi_i\, s_{ir}(\hat{r},0) \qquad (18)$$

where $S_{i0}(\hat{r}) = S_i(\hat{r},0)$ and χ may be a function of $\hat{r}$.

It must be pointed out that calculations were also performed by solving for three components of a diagonal molecular orientation tensor in order to verify that the numerical errors in the calculation of the trace were small. This was indeed the case when the initial conditions for the radial component were identical to those for the azimuthal one.

The dynamic viscosity is

$$\hat{\mu}_{ei,0} = \hat{\mu}_{i,0} \cdot \exp\left(\beta_i\left(\frac{Y_i}{Y_{\infty,i}}\right)^{n_i}\right) + \frac{2}{3}\alpha_i\,\lambda_i\,S_i^2$$

where $\hat{\mu}_{i,0} = G_i \exp(E_i \cdot (1-\hat{T}_i))$ denotes the linearized form of the Arrhenius dependence of the dynamic viscosity on temperature where G and E denote the nondimensional pre-exponential factor and activation energy, respectively.

The formulation presented here is also valid for amorphous compound fibers which are characterized by $\mathbf{S}_i=\mathbf{0}$ and $\beta_i = 0$ and, therefore, the effective dynamic viscosity only depends on temperature.

It must be noted that the linearization of the Arrhenius expressions for the dynamic viscosity law and the relaxation time are really linearization of the argument of the exponential rather than the linearization of the whole Arrhenius law, i.e., in the expression $C\exp(-T_a/T)$ where T_a and C are constants, the linearization of the argument of the exponential about T_m yields $C\exp(-T_a/T_m)$ $\cdot\exp(T_a(T_m-T)/T_m^2)$ and, therefore, $E = T_a/T_m$ and $G = C\exp(T_a/T_m)$ if $T_0 = T_m$.

Equations (13) and (14) indicate that the molecular orientation depends on the axial derivative of the leading-order axial velocity, i.e., it depends on the axial elongation rate, and, therefore, molecular orientation in the axial direction is enhanced.

Equation (11) indicates that the molecular orientation affects the crystallization in an exponential manner through $k_{Ai}(S)$, and the crystallization, temperature and molecular orientation are coupled through the viscosity which, in turn, is affected by the temperature field and affects the fiber's geometry and its properties. On the other hand Eqs. (13) and (14) show that the diagonal molecular orientation tensor used in this study depends on the leading-order axial strain rate and on the temperature through the relaxation time.

It must be noted that, if the second term in the right hand-sides of Eqs. (13) and (14) are neglected, and these equations are interpreted in Lagrangian coordinates, they have the following critical points $(s_{ir}, s_{ix}) = (\gamma_r, -1)$ and $(1,2)$; the latter corresponds to the following diagonal molecular orientation tensor

$$\mathbf{S}=\frac{1}{3}\begin{pmatrix} -1 & 0 & 0 \\ 0 & -1 & 0 \\ 0 & 0 & 2 \end{pmatrix}, \qquad (19)$$

which is proportional to the leading-order velocity gradient tensor and coincides with molecular orientation tensor used by Forest et al. [10]. These authors used an equation for the order parameter rather than the two equations employed here for the *rr* and *xx* components of the diagonal molecular orientation tensor.

Since the dynamic viscosity depends on the two-dimensional fields of $\hat{T}$, Y and S, the dynamic viscosity that appears in Eqs. (5)–(6) and (8)–(9) is

$$<\hat{\mu}_{e1,0}>(\hat{x}) = \int_{R_1}^{R_0} \hat{\mu}_{e1,0}(\hat{r},\hat{x})\,\hat{r}\,d\hat{r} / A_1\,, \qquad (20)$$

$$<\hat{\mu}_{e2,0}>(\hat{x}) = \int_{R_0}^{R_2} \hat{\mu}_{e2,0}(\hat{r},\hat{x})\,\hat{r}\,d\hat{r} / A_2\,, \qquad (21)$$

and the integrals that appear in these averaged dynamic viscosities provide an integro-differential character to the melt spinning of hollow, compound semi-crystalline fibers governed by the quasi-one-dimensional model given by Eqs. (4), (6), (7), (10), (11), and (13)–(14).

It should be emphasize that the model for the melt spinning of compound fibers presented here is a

single-phase, single-component one characterized by a Newtonian rheology and which does not account for latent heat effects associated with solidification; neither does it account for the presence of amorphous and crystalline phases in a separate manner either through conservation equations for these components or through a non-Newtonian rheology. Although the latent heat effects associated with phase changes may result in a locally small increase of temperature at the solidification point, they are usually small in melt spinning; on the other hand, the non-Newtonian rheology of semi-crystalline compound jets may have an important influence on the fluid dynamics, heat transfer, molecular orientation and crystallization of such fibers.

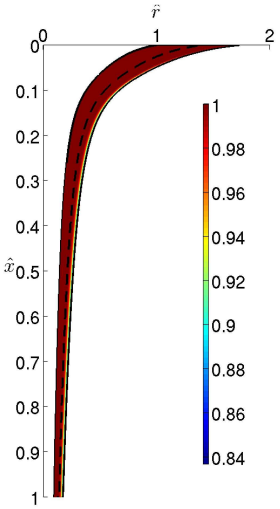

Figure 2
Temperature distribution in the hollow compound fiber.

RESULTS AND DISCUSSION

The equations of the quasi-two-dimensional model presented in the previous section were solved for steady-state fibers in meshes consisting of 1001 grid points in the axial direction, and 101 grid points for each jet in the radial one. For the numerical solution of the two-dimensional energy, molecular orientation parameter and degree of crystallization, the non-dimensional physical domain of the hollow compound fiber $(\hat{r},\hat{x})$ was mapped into two rectangular domains one each for the inner and outer jets $(\xi,\eta)=\left((\hat{r}^2-R_1^2)/(R_2^2-R_1^2),\,\hat{x}\right)$ so that the interface between the inner and outer jets is located at $V_1/(V_1+V_2)$ and that between the outer one and its surroundings is located at 1, where V_1 and V_2 is the (nondimensional) volumetric flow of the inner jet and outer jets, respectively.

The leading-order axial momentum equations and the two-dimensional equations for the energy, molecular orientation and degree of crystallization were solved iteratively by means of central differences in space for the diffusion-like terms and first-order upwind differences for the advection-like ones, until convergence was achieved. In all the calculations, the solution of the leading-order one-dimensional equations for slender hollow compound fibers was used as initial guess and convergence was reached when the L_2-norm of the difference between the solutions corresponding to two successive iterations was less than or equal to 10^{-8}.

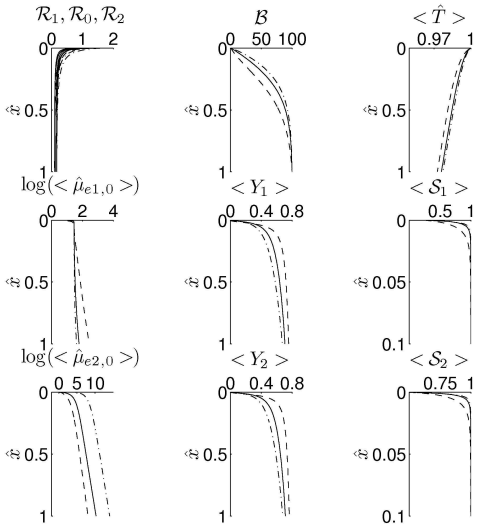

Figure 3
Hollow compound fiber's geometry (top left), leading-order axial velocity (top middle), cross-sectional averaged temperature (top right), cross-sectional averaged dynamic viscosity (left), cross-sectional averaged molecular orientation parameter (middle) and cross-sectional averaged degree of crystallization (right) as functions of the axial distance along the fiber. Solid line: G_2=1, dashed line: G_2=0.01; dashed-dotted line: G_2=100.

Unless otherwise stated, the results presented in this section correspond to $\overline{R}=1$, and $\overline{R}/\overline{F}=1$, $\overline{P}=100$, $\overline{C}=1$, $\overline{B}=10$, $\overline{b}=0$, $E_i=100$, $\hat{\rho}_i=\hat{C}_i=\hat{K}_i=1$, $\hat{h}_2=1$, $\sigma_i/\sigma=1$, $G_i=1$, $\beta_i=1$, $n_i=4$, $\alpha_i=5$, $\hat{\lambda}_{i,0}=1$, $\omega_i=0$, $\psi_i=0.5$, $N_i=4$, $k_{Ai}(0)=0.005$, $a_{2i}=10$, $Y_{i,\infty}=0.8$, $V_i=0.5$, $B(0)=1$, $B(1)=100$, $\hat{T}_i(\hat{r},0)=1$,

$T_{2,\infty}=0$, $S_1(\hat{r},0)=0.25$, $S_2(\hat{r},0)=0.50$, $\chi_i=2$, and $Y_i(\hat{r},0)=0$.

Some sample results are illustrated in Figure 2 which clearly indicates that a thermal boundary layer is formed at the fiber's outer radius due to heat exchanges with the surroundings. Since adiabatic conditions were imposed at the fiber's inner radii, no boundary layer is observed at that interface.

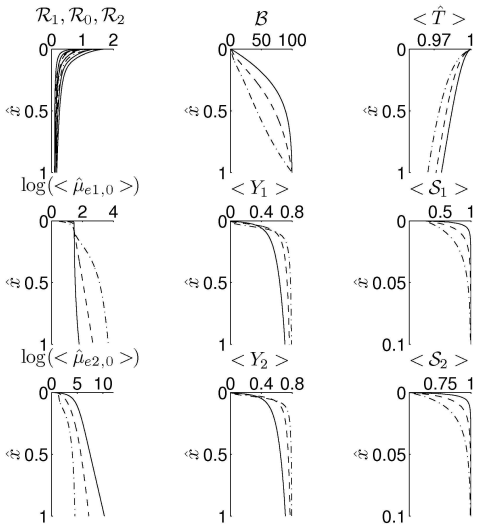

Figure 4
Hollow compound fiber's geometry (top left), leading- order axial velocity (top middle), cross-sectional averaged temperature (top right), cross-sectional averaged dynamic viscosity (left), cross-sectional averaged molecular orientation parameter (middle) and cross-sectional averaged degree of crystallization (right) as functions of the axial distance along the fiber. Solid line: E_2=100, dashed line: E_2=50; dashed-dotted line: E_2= 10.

Figure 3 indicates that the three radii of the hollow compound fiber are monotonically decreasing functions of the axial distance along the fiber and that there is a great contraction at the beginning. This figure also shows that, depending on the pre-exponential factor in the Arrhenius dependence of the outer jet's dynamic viscosity on the temperature, G_2, the leading-order axial velocity B may exhibit a one-sign curvature for $G_2=1$ and 100, or a two-sign curvature for $G_2=0.01$. The nondimensional cross-sectional averaged temperature is higher for $G_2\geq 1$ than for $G_2<1$; the leading-order axial velocity component at a given axial location is higher except at the die's exit and take-up point for $G_2\geq 1$ than for $G_2<1$, in accord with the linearized Arrhenius dependence of the dynamic viscosity on temperature employed in this study. Figure 3 also indicates that the cross-sectional averaged viscosity of the outer jet increases at a greater pace for $G_2\geq 1$ than that at the inner one due to heat transfer losses; the degree of molecular orientation increases as G_2 is decreased and reaches rapidly at constant value, whereas the degree of crystallization is similar for the inner and outer jets, tends to its (specified) ultimate value and decreases as G_2 is increased. Since the heat transfer losses decrease as G_2 is increased, this result indicates that, for the cases considered in Figure 3, flow-induced crystallization is important, at least, for high values of the pre-exponential factor of the Arrhenius viscosity law.

Although not shown here, the fiber's geometry, molecular orientation and crystallization were found to be nearly independent of the activation energy of the dynamic viscosity law for $50\leq E_1\leq 100$ and $E_2=100$, and were found to be similar to those corresponding to $G_2=1$ in Figure 3 and are consistent with the fact that heat exchanges with the surroundings only occur at the outer jet's outer interface. On the other hand, for $10\leq E_2\leq 100$ and $E_1=100$, substantial differences are observed in the axial velocity profiles as indicated in Figure 4; these differences are somewhat expected because only the activation energy of the outer jet's dynamic viscosity law is varied and heat losses only occur at the outer jet's outer interface. Figure 4 also indicates that depending on the heat transfer rate at the outer radius of the outer material and the activation energy of the viscosity law of the outer jet, the axial velocity may be concave upwards from the die's exit to the take-up point or concave upwards first and then concave downwards later and reaches a constant value once the fiber solidifies. Of the three axial velocity profiles shown in Figure 4, only the one associated with the solid line corresponds to a complete solidification, and this solidification is, in turn, associated with a large increase in the dynamic viscosity. Figure 4 also shows that the averaged dynamic viscosity of the compound fiber, i.e., $(<\hat{\mu}_{e1,0}>A_1+<\hat{\mu}_{e2,0}>A_2)/(A_1+A_2)$, increases with axial distance on account of the temperature drop and complete solidification may be reached.

Figure 4 also indicates that the dynamic viscosity increases quite rapidly at the beginning due to flow straining and may continue increasing if the fiber does not solidify before being drawn at the take-up point. The degree of solidification also increases quite rapidly at the beginning where flow straining is largest.

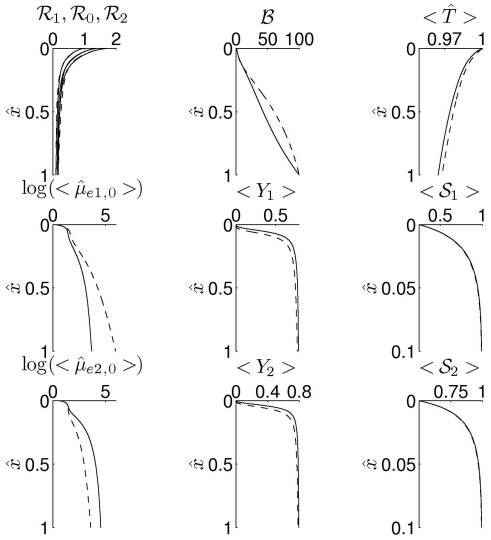

Figure 5
Hollow compound fiber's geometry (top left), leading-order axial velocity (top middle), cross-sectional averaged temperature (top right), cross-sectional averaged dynamic viscosity (left), cross-sectional averaged molecular orientation parameter (middle) and cross-sectional averaged degree of crystallization (right) as functions of the axial distance along the fiber. Solid line: quasi-two-dimensional model; dashed line: one-dimensional model.

The quasi-two-dimensional model of the melt spinning of hollow compound fibers presented in this study uses the leading-order equations obtained from an asymptotic analysis of slender fibers at low Reynolds and Biot numbers, and the two-dimensional equations for the energy, molecular orientation and crystallization, but no small Biot number approximation is made on the two-dimensional energy equation. This seemingly contradictory approximation raises the following question: how do the results of the quasi-two-dimensional model presented here compared with those of the one-dimensional model for low Reynolds and Biot numbers. The differences between these two models are illustrated in Figure 5 which corresponds to the same parameters as those of Figure 2. It must be noted that the cross-sectionally averaged temperature, order parameter for molecular orientation and degree of crystallization of the quasi-to-dimensional model are presented.

Figure 5 indicates that the averaged temperature predicted by the quasi-two-dimensional model is slightly lower than the temperature predicted by one-dimensional one, whereas the two-dimensional model predicts a one-sign curvature axial velocity component and the one-dimensional one predicts a two-sign curvature. These differences are mainly due to the temperature distribution across the fiber, for, whereas the one-dimensional model predicts a uniform temperature across the fiber, the quasi-two-dimensional one indicates that a thermal boundary layer is formed at the outer jet's outer interface.

Figure 5 also shows that there are very few differences in the molecular orientation predicted by the one- and quasi-two-dimensional models and this is due to the dependence of the order parameter on the axial strain rate and the fact that there is a large contraction near $\hat{x} = 0$. There are, however, some differences in the degree of crystallization, e.g., the quasi-two-dimensional model predicts a shorter distance for achieving full crystallization than the one-dimensional one, and these differences are mainly due to the temperature differences between these two models and the radial velocity component in the two-dimensional one, because, as indicated above, the crystallization kinetics employed in this study depends mainly on temperature through the axial velocity component in its advection terms in the axial and radial directions, and exponentially on the order parameter for the molecular orientation. Since almost complete orientation is achieved shortly after $\hat{x} = 0$, the characteristic distance for achieving full crystallization is inversely proportional to the velocity along the streamlines; since the velocity in the radial direction is largest near $\hat{x} = 0$, it is expected that the crystallization of the two-dimensional model be larger than that of the one-dimensional one, at least, initially, in accord with the results presented in Figure 5. Furthermore, the equations for the models of molecular orientation and crystallization are of the hyperbolic type and, therefore, may predict different values of these variables at the core-cladding interface. However, physical considerations indicate that, at that interface, there would be entanglements between the polymeric molecules of the inner and outer jets and a transition region may be appear there; such a transition region should, in turn, affect

the crystallization of the two fluids and their temperatures and velocities, at least, locally. Molecular entanglement at that interface has not been considered in the model presented here.

CONCLUSIONS

A quasi-two-dimensional model of the melt spinning of hollow compound fibers for Newtonian fluids which includes the molecular orientation and crystallization has been presented. The model uses the one-dimensional leading-order equations for the fiber's geometry and axial velocity components obtained from an asymptotic analysis for slender fibers at low Reynolds numbers together with two-dimensional equations for the thermal energy and the degrees of molecular orientation and crystallization. The crystallization has been modeled through the Avrami-Kolmogorov thermal kinetics but includes flow-induced crystallization through the strain rate tensor and the molecular orientation. The Doi-Edwards transport equation for the molecular orientation tensor has been employed albeit simplified to a scalar order parameter.

It has been shown that, because of the nonlinear coupling between the variables, the exponential dependence of the dynamic viscosity on temperature and the use of a leading-order equation for the axial momentum, the model is integro-differential and its results are highly dependent on the pre-exponential factor and activation energy of the Arrhenius law used to define the dynamic viscosity of the outer jet. It has also been found that almost complete molecular orientation is achieved near the die's exit, solidification of the hollow compound fiber is mainly associated with the large increase of viscosity as the temperature decreases, the degree of crystallization increases along the fiber and tends to its ultimate value; whether this ultimate crystallization is or is not achieved depends on the fiber's cooling and viscosity.

ACKNOWLEDGMENTS

The research reported in this paper was supported by Project FIS2009-12894 from the Ministerio de Ciencia e Innovación of Spain and fondos FEDER.

REFERENCES

1. Zubia, J, and Arrue, J, 2001, Plastic optical fibers: An introduction to their technological processes, Opt. Fiber Technol., **7**, pp. 101-140.
2. Pone, E Dubois, C, Guo, N, Lacroix, S, and Skorogatiy, M, 2006, Newtonian and non–Newtonian models of the hollow all-polymer Bragg fiber drawing, J. Lightwave Technol., **24**, pp. 4991-4999.
3. Ramos, J. I, 1999, Asymptotic analysis of compound liquid jets at low Reynolds numbers, Appl. Math. Comput., **100**, pp. 223-240.
4. Fitt, A. D, Kurusawa, K, Monro, T. M, Please, C. P, and Richardson, D. J, 2002, The mathematical modelling of capillary drawing for holey fibre manufacturing, J. Eng. Math., **43**, pp. 201-227.
5. Voyce, C. J, Fitt, A. D, and Monro, T. M, 2004, Mathematical model of the spinning of microstructured fibres, Opt. Express, **12**, pp. 5810-5820.
6. Xue, S. C, Tanner, R. I, Barton, G. W, Lwin, R, Large, M. C. J, and Poladian, L, 2005, Fabrication of microstructured optical fibers–Part I: Problem formulation and numerical modeling of transient draw process, J. Lightwave Technol., **23**, pp. 2245-2254.
7. Xue, S. C, Tanner, R. I, Barton, G. W, Lwin, R, Large, M. C. J, and Poladian, L, 2005, Fabrication of microstructured optical fibers–Part II: Numerical modeling of steady–state draw process, J. Lightwave Technol., **23**, pp. 2255-2266.
8. Ramos, J. I, 2001, Nonlinear dynamics of hollow, compound jets at low Reynolds numbers, Int. J. Eng. Sci., **39**, pp. 1289-1314.
9. Ramos, J. I, 2005, Convection and radiation effects in hollow, compound optical fibers, Int. J. Therm. Sci., **44**, pp. 832-850.
10. Forest, M. G, Zhou, H, andWang, Q, 2000, Thermotropic liquid crystalline polymer fibers, SIAM J. Appl. Math., **60**, pp. 1177-1204.
11. Ziabicki, A, 1976, *Fundamentals of Fibre Formation* John Wiley & Sons, New York.